



Numerical Modeling of a Stenosed Artery Using Mathematical Model of Variable Shape

S. Mukhopadhyay

Department of Mathematics
M.U.C. Women's College
Burdwan-713104, W. B., India
swati_bumath@yahoo.co.in

G. C. Layek*

Department of Mathematics
The University of Burdwan
Burdwan-713104, W.B., India
glayek@yahoo.com

*Author for correspondence

Received: January 29, 2008; Accepted: June 23, 2008

Abstract

The intention of the present work is to carry out a systematic analysis of flow behavior in a two-dimensional tube (modeled as artery) with a locally variable shaped constrictions. The simulated artery, containing a viscous incompressible fluid representing the flowing blood, is treated to be complaint as well as rigid tube. The shape of the stenosis in the arterial lumen is chosen to be symmetric as well as asymmetric about the middle cross section perpendicular to the axis of the tube in order to improve resemblance to the in-vivo situation. The constricted tube is transformed into a straight tube and the resulting governing equations are solved by a numerical method with Reynolds number and 'n', a number giving the shape of the constriction as parameters. The influences of these parameters on the haemodynamic factors like wall shear stress, pressure and velocity have been analyzed. The present findings demonstrate that the flow resistance decreases as the shape of a smooth stenosis changes and maximum resistance is attained in case of a symmetric stenosis. But the length of separation increases in case of asymmetric constrictions and the oscillation in the shear layer appears earlier in case of asymmetric constriction than that in the case of symmetric constriction. Maximum resistance is attained in case of rigid stenosed tube rather than the flexible one.

Key words: Axi-symmetric flow, stenosis of variable shape, two-dimensional model, staggered grid, finite difference scheme

MSC: 76Dxx, 74S20

1. Introduction

Atherosclerosis is a disease which severely influences human health. It is characterized by the hardening and thickening of the arterial walls due to the formation of plaque. With the progress of disease, the formation of plaque reduces the arterial passage area creating uncharacteristic blood flow patterns. As a result, this restriction, if severe enough, can cause individuals to suffer cardiac arrest or stroke. Stenoses have a complex influence on haemodynamics through and beyond the narrowed arterial segment. Atherosclerotic disease tends to be localized in regions of geometrical irregularity such as vessel branch, curved and tapered arteries and stenotic sites. Coronary artery disease which is the largest single cause of mortality in developed nations, occurs when the coronary arteries narrow to such an extent that they are unable to transport sufficient blood to the heart muscle for it to function efficiently. The two main causes of death from coronary artery disease are rupture of the plaque causing sudden occlusion of the artery and the slow build up of a stenosis in the artery due to atherosclerosis. Reduction in blood flow caused by stenosis build up also causes debilitation.

In order to have a complete understanding of the development of the stenosis from the physiological point of view, one needs to be fully conversant with the haemodynamic behavior of the streaming blood together with the mechanical properties of the vascular wall material under physiological conditions. The ability to describe the flow through stenosed vessels would provide the possibility of diagnosing the disease in the earlier stages, even before the stenosis become clinically relevant, and is the basis for surgical intervention. Appropriate and timely intervention by cardiologists greatly reduces the risk of death. Mathematical modeling to predict flow through atherosclerotic arteries augment the perception and experience of cardiologists and assist understanding of the genesis and progression of stenosis development. Such techniques allow to predict the haemodynamic characteristics as pressure, shear stress, velocity and reduction in flow.

Experimentally based models of blood flow rely on empirical data collected by invasive or non-invasive means. Both types of data collection have their problems. The inaccuracies introduced by interactions between the apparatus and the blood are considerably greater than the quantities being measured in atherosclerotic coronary arteries. Mathematical modeling provides an economical and non-invasive method of studying blood flow through arteries. Two approaches: analytical and computational are used. Analytical methods are best studied to explore the underlying physics of the situation and to provide real time results for simplified situations. Computational fluid dynamic modeling is one of the powerful means to analyze the blood flow because we can incorporate the complex nature of blood flow and the blood vessel interactions into the study.

In the recent past quite a good number of theoretical and experimental investigations related to blood flow in arteries in the presence of stenosis have been carried out with various perspectives in the realm of arterial biomechanics. Some attempts to study experimentally steady and unsteady flows across a smooth stenosis can be found in Young and Tsai (1973), Ahmed and Giddens (1983) etc. For single constriction flow, numerical research investigations are numerous Deshpande, et al. (1976), Mishra and Chakravarty (1986), Pontrelli (2001).

In reality, this is not generally the case. Arterial stenosis contain many ups and downs and the shape is also of asymmetric pattern. In general, the surface irregularities and the asymmetric shape of the constriction cause complexity in performing experimental and numerical simulations of the flow phenomena. Some sincere attempts have already been made to investigate the flow characteristics through vessels with such type of occlusion Back, et al. (1984), Johnston and Kilpatrick (1991), Andersson, et. al. (2000), Chakravorty, et al. (2005). The disturbances created by the constriction are in the post-stenotic region. The pressure loss in the post-stenotic region can reduce the supply of blood through the artery and also impose additional load on the heart. The pressure losses are significant when the internal diameter is reduced beyond 50% of the nominal value Young (1979). Wall Pressure and shear stress play an important role in case of fluctuations of the flow variables in the blood flow downstream of the stenosis. This can damage and weaken the internal wall (intima) of the artery. The post-stenotic dilatation i.e., widening of the artery in the downstream of the stenosis is due to the increased distensibility of the arterial wall induced by the variation of pressure Roach (1963), Lighthill (1975). Furthermore, the variability in the distal arterial wall shear stress can result in a predilection towards atherosclerosis.

The rheology of blood can best be described by Casson's relationship and the blood exhibits non-linear shear stress vs rate of shear characteristics especially at low rates of shear. But at relatively high rates of shear, the viscosity coefficient asymptotically approaches a constant value. Hence, for flow in a large blood vessels, where relatively large shear rates can be expected (during systole), a Newtonian description appears to be reasonable. Blood flow in the larger vessels can be modeled quite accurately as a Newtonian fluid Pedley (1980), Fung (1981).

Keeping this fact in mind, we investigated the flow pattern in a tube with single constriction. A novel mathematical description of the compliant wall geometry (given by time dependent equation) is used in this study to provide more realistic model of the wall by giving both symmetric as well as asymmetric (about the middle cross section perpendicular to the axis of the tube) stenosis-geometry. We have also considered the shape of stenosis geometry as depicted by the data collected from a casting of a left circumflex coronary artery with mild, diffuse atherosclerotic disease for the validation of our numerical code. When stenoses develop in human vasculature, the vessel walls in the vicinity of the stenosis are usually relatively solid but when the distensibility of the vessel wall is inducted, they will no longer be rigid. For a flexible vessel, the stenosis can not remain static and this feature is quite relevant to the unsteady flow mechanism under stenotic condition. A stable two-stage numerical scheme has been developed for this problem in the axi-symmetric approximations. The staggered grid and the finite difference discretizations are employed in the present scheme. The flow reached steady state after a sufficiently long time. Due attention has been paid on wall shear stress, pressure distribution, velocity profiles etc.

2. Equations of motion

We consider an axi-symmetric and laminar separated flow in a constricted tube, constricted at the specified position. The blood flow through an axi-symmetric stenosis can be simulated in two-dimensions by making use of cylindrical co-ordinate system. Let (r^*, θ^*, z^*) be the

cylindrical polar co-ordinates with z^* -axis along the axis of symmetry of the tube. The region of interest is $0 \leq r^* \leq r_0(z^*)$, $0 \leq z^* \leq L^*$ (L^* being the finite length of the tube). The incompressible two-dimensional Navier-stokes equations can be taken for the modeling of Newtonian blood flow past multiple constrictions. Let u^* and v^* be the axial and radial velocity components respectively, p^* the fluid pressure, ρ the constant density and ν denotes the kinematic viscosity of the fluid. Let U be the maximum inflow velocity specified in the inlet section or test section of the tube. We introduce the non-dimensional variables $t = t^*U/D_0$, $r = r^*/D_0$, $z = z^*/D_0$, $r_0(z) = r_0^*(z^*/D_0)/D_0$, $u = u^*/U$, $v = v^*/U$, $p = p^*/\rho U^2$ where D_0 is the diameter of tube in the unoccluded portion. The governing equations for incompressible fluid flow representing conservation of mass and momentum fluxes may be expressed in dimensionless variables as

$$r \frac{\partial u}{\partial z} + \frac{\partial v r}{\partial r} = 0, \quad (1)$$

$$\frac{\partial u}{\partial t} + \frac{\partial u v}{\partial r} + \frac{\partial u^2}{\partial z} + \frac{u v}{r} = -\frac{\partial p}{\partial z} + \frac{1}{\text{Re}} \left[\frac{\partial^2 u}{\partial r^2} + \frac{1}{r} \frac{\partial u}{\partial r} + \frac{\partial^2 u}{\partial z^2} \right], \quad (2)$$

$$\frac{\partial v}{\partial t} + \frac{\partial v^2}{\partial r} + \frac{\partial u v}{\partial z} + \frac{v^2}{r} = -\frac{\partial p}{\partial r} + \frac{1}{\text{Re}} \left[\frac{\partial^2 v}{\partial r^2} + \frac{1}{r} \frac{\partial v}{\partial r} + \frac{\partial^2 v}{\partial z^2} - \frac{v}{r^2} \right], \quad (3)$$

where $\text{Re} = UD_0/\nu$ is the Reynolds number.

2.1. Boundary conditions

Along the axis of symmetry, the normal component of velocity and shear stress vanish so that

$$\frac{\partial u(z, r, t)}{\partial r} = 0, \quad v(z, r, t) = 0 \quad \text{on } r = 0. \quad (4)$$

The velocity boundary conditions on the arterial wall when treated to be rigid are the usual no-slip conditions given by

$$u(z, r, t) = v(z, r, t) = 0 \quad \text{at } r = r_0(z), \quad (5a)$$

while those in the case of flexible wall are

$$u(z, r, t) = 0, v(z, r, t) = \frac{\partial r_0(z, t)}{\partial t} \quad \text{on } r = r_0(z, t). \quad (5b)$$

The governing equations of our model assume that the flow regime is laminar. This model also assumes the flow to be fully developed at the inlet test section of the tube where the inlet section is considered at the position $z=0$. The inlet velocity conditions are assumed to have a parabolic profile corresponding to Hagen-Poiseuille flow through a long circular tube as

$$u(z, r, t) = 2(1-r^2), \quad v(z, r, t) = 0 \text{ at } Z = 0. \quad (6)$$

The downstream length (60) [see Fig.1(a)] is sufficiently long so that the reattachment length is independent of the length of calculation domain. The zero velocity gradient boundary conditions are used at the outlet cross-section of the tube

$$\frac{\partial u(z, r, t)}{\partial z} = 0, \quad \frac{\partial v(z, r, t)}{\partial z} = 0. \quad (7)$$

2.2. Initial condition

The initial condition is that there is no flow inside the region of the tube except the parabolic velocity profile at the inlet. The flow is gradually developing as time elapses.

2.3. Transformation of basic equations

We consider a co-ordinate stretching in the radial direction which transforms the constricted tube into a straight circular tube, given by

$$R = \frac{r}{r_0(z)}, \quad 0 < r < r_0 \quad (8)$$

where the function $r_0(z)$ is defined as

$$r_0(z) = \begin{cases} L_0 [1 - A_0 \{l^{n-1}(z-\alpha) - (z-\alpha)^n\}], & \alpha \leq z \leq \beta \\ L_0, & \text{otherwise.} \end{cases} \quad (9)$$

Here $r_0(z)$ denotes the radius of the tube in the constricted region. Here α is the distance from the start of the segment to the start of the stenosis, β is the distance from the start of the segment to the end of the stenosis, n (≥ 2) is a parameter determining the shape of the stenosis, l is the length of the stenosis, L_0 is the unstricted radius of the tube. Here the constant A_0 is given by

$$A_0 = \frac{h}{L_0 l^n} \frac{n^{\frac{n}{n-1}}}{n-1},$$

where h is the height of the stenosis.

All the profiles, given by equation (9) appear to be time-independent (rigid) and their time-dependence can easily be introduced in such a way that $r_0(z, t) = r_0(z) \cdot a_1(t)$ where $a_1(t) = 1 + k \cos(\omega t - \phi)$ with the amplitude parameter k , the phase angle ϕ and the angular frequency ω .

A schematic diagram of the differently shaped constricted tube geometry considered in this analysis is given in Fig.1(a) along with all relevant quantities. The tube under consideration is

taken to be of finite length 60 for low Reynolds number flow. But suitable length is taken for the case of high Reynolds numbers so that the reattachment length is independent of this downstream distance. In the present study, we have taken $n = 2, 4, 6$ so that the symmetric (about its center), slightly asymmetric and severely asymmetric constrictions of width 14 are developed respectively.

3. Numerical computations

The transformed governing equations for viscous, incompressible fluid flows are discretized using finite-difference approximations. The well known staggered grid proposed by Harlow and Welch (1965) is used in the present work. Discretization of the continuity equation at (i,j) cell delivers

$$R_j r_0(z_i) \frac{u_{i,j}^n - u_{i-1,j}^n}{\delta z} - R_j^2 \frac{\partial r_0(z_i)}{\partial z} \frac{utc - ubc}{\delta R} + \frac{Rl_j v_{i,j}^n - Rl_{j-1} v_{i,j-1}^n}{\delta R} = 0 \quad (10)$$

where utc, ubc are defined as follows.

$$\begin{aligned} utc &= 0.25 (u_{i,j}^n + u_{i-1,j}^n + u_{i-1,j+1}^n + u_{i,j+1}^n), \\ ubc &= 0.25 (u_{i,j}^n + u_{i-1,j}^n + u_{i,j-1}^n + u_{i-1,j-1}^n). \end{aligned}$$

Considering the source, convective and diffusive terms at the n^{th} time level, the momentum equation in Z -direction in finite difference form may be put as

$$\frac{u_{i,j}^{(n+1)} - u_{i,j}^n}{\delta t} = \frac{p_{i,j}^n - p_{i+1,j}^n}{\delta z} + \frac{R_j}{r_0(zl_i)} \frac{\partial r_0(zl_i)}{\partial z} \frac{pt - pb}{\delta R} + Ucd_{i,j}^n \quad (11)$$

where the terms pt, pb and $Ucd_{i,j}^n$ are defined as follows:

$$\begin{aligned} pt &= 0.25(p_{i,j}^n + p_{i+1,j}^n + p_{i,j+1}^n + p_{i+1,j+1}^n), \\ pb &= 0.25(p_{i,j}^n + p_{i+1,j}^n + p_{i,j-1}^n + p_{i+1,j-1}^n), \\ Ucd_{i,j}^n &= \frac{1}{Re} Diffu_{i,j}^n - Conu_{i,j}^n. \end{aligned}$$

The finite difference equation approximating the momentum equation in the R -direction is

$$\frac{v_{i,j}^{(n+1)} - v_{i,j}^n}{\delta t} = \frac{1}{r_0(z)} \frac{p_{i,j}^n - p_{i,j+1}^n}{\delta R} + Vcd_{i,j}^n \quad (12)$$

where

$$Vcd_{i,j}^n = \frac{1}{Re} Diffv_{i,j}^n - Conv_{i,j}^n.$$

Here $Vcd_{i,j}^n$ is the Discretization of convective and diffusive terms of U -momentum equation at the n -th time level at cell (i, j) . The diffusive and the convective terms in the U -momentum equation are differenced similar to that in u -momentum for the convective flux. The Poisson equation for pressure is obtained by combining the discretized form of the momentum and continuity equation. The final form of the Poisson equation for pressure is

$$\begin{aligned} & (A + B + C + D)p_{i,j}^n - Ap_{i+1,j}^n - Bp_{i-1,j}^n + A_1p_{i+1,j+1}^n - A_1p_{i+1,j-1}^n \\ & - A_2p_{i-1,j+1}^n + A_2p_{i-1,j-1}^n - (C - A_1 + A_2)p_{i,j+1}^n - (D + A_1 - A_2)p_{i,j-1}^n \\ & = - \left[\frac{Di v_{i,j}^n}{\delta t} + R_j r_0(z_i) \frac{Ucd_{i,j}^n - Ucd_{i-1,j}^n}{\delta z} + \frac{Rl_j Vcd_{i,j}^n - Rl_{j-1} Vcd_{i,j-1}^n}{\delta R} \right] \end{aligned} \quad (13)$$

where A, B, C, D, A_1, A_2 all are given in Layek, et al. (2005). Here $Di v_{i,j}^n$ is the finite-difference representation of the divergence of the velocity field at cell (i, j) .

Then the final form of Poisson equation is solved iteratively with the help of appropriate boundary conditions and then the pressure-velocity correction formulae are invoked until we achieve a satisfactory level of divergence value.

3.1. Stability criteria of the scheme

The time-step (δt) is calculated by the two criteria given below. First the fluid can not move through more than one cell in one time step (Courant, Friedrichs and Lewy condition). So, the time step must satisfy the following criteria

$$\delta t \leq \text{Min} \left[\frac{\delta z}{|u|}, \frac{\delta R}{|v|} \right]_{ij}, \quad (14)$$

where minimum is taken in the global sense. Secondly, momentum must not diffuse more than one cell in one time step. This condition, which is related to the viscous effects, implies

$$\delta t \leq \text{Min} \left[\frac{\text{Re}}{2} \frac{\delta z^2 \delta R^2}{(\delta z^2 + \delta R^2)} \right]_{ij}. \quad (15)$$

Denoting the right hand side of (14) and (15) by δt_1 and δt_2 respectively we find that both these inequalities are satisfied if the time step δt satisfies

$$\delta t \leq \text{Min} [\delta t_1, \delta t_2], \quad (16)$$

Hence, in our computations we take

$$\delta t = c \text{Min} [\delta t_1, \delta t_2], \quad (17)$$

where c is a constant lying between 0.2 to 0.4. A typical value of δt is 0.005 for $\delta z = 0.05$ and $\delta R = 0.05$.

4. Results and discussions

For the purpose of numerical computation of the desired quantities of major physiological significance, numerical values of the specific geometry of the stenosed artery considered for simulations and the parameters involved in this study have been ranged around some typical values in order to obtain results of physiological interest:

$$\alpha = 10, \beta = 24, l = 14, L_0 = \frac{D_0}{2} = 1, n = 2(4,6), h = 0.3(0.5), k = 0.001,$$

$$\omega = 2\pi \times 1.2 \text{ Hz}, \phi = 180^\circ.$$

The computed results are obtained following the above mentioned numerical scheme [taking $\delta t = 0.005$ for $\delta z = 0.05$ and $\delta R = 0.05$] for various physical quantities of major physiological significance. In order to have their quantitative measures they are all exhibited through the figures 3-11 and discussed at length.

Arterial constriction, whilst having the general trend of smooth curve, contains many small valleys and ridges, analogous to mountain range. For the purpose of deeper investigation into this problem, the published data Back, et al. (1984) are used to define the outline of the stenosis Fig.1(b). To compare our results with Back, et al. (1984), Johnston and Kilpatrick (1991), Andersson, et al. (2000), the arterial wall distensibility is disregarded in some cases but attention also has been paid on compliant wall model.

A comparison of wall shear stress is made (see Fig.2(a)) with the present results obtained using a two-stage numerical scheme for the case of asymmetric single constriction with irregular surface geometry (see Fig.1(b)) for the Reynolds numbers $Re=20$ and $Re=1000$. Our results agree well with that of Johnston and Kilpatrick (1991).

The present results involving the pressure drop in case of irregular stenosis for different Reynolds number from 10 to 1000 are compared with the numerical results of Andersson, et al. (2000) and the experimental results of Back, et al. (1984) in Fig.2(b). The comparison in Fig.2(b) shows considerable agreement with the experimental results of Back, et al. (1984). But there is a little variation with the numerical results of Andersson, et al. (2000). It seems that the unsteady flow mechanism of the present investigation is responsible for this.

In presence of a narrowing i.e. a constriction, the flow exhibits a resistance and hence an increase of the shear stress (i.e., the wall vorticity) and a pressure drop. These are quantities of physiological relevance.

Wall pressure distribution is very much important because the post-stenotic dilatation due to arterial damage is caused by the variation of pressure associated with the complex flow structure. Pressure fluctuations on the arterial wall produce acoustic signals that can be detected externally Mittal, et al. (2001).

A rapid fall in pressure is observed (Fig.3) as the occlusion is approached and the local minimum is attained corresponding to the separation point in case of symmetric and asymmetric constrictions ($n = 2$ & 4). The two curves are of similar nature and the comparing pressure distribution curves over the two stenoses (symmetric and asymmetric) show that the asymmetric stenosis predicts higher values than the symmetric stenosis (Fig.3). With increasing degree of stenosis, the reduction in pressure at the throat decreases significantly in case of symmetric as well as asymmetric constrictions.

Fig.4 exhibits the variation of center line velocity in axial direction at $Re = 600$ for differently shaped stenoses (taking $n = 2, 4$ & 6). It is very clear from the figure that the maximum centre line velocity occurs slightly in the downstream of the constriction due to formation of recirculation zone near the wall as a result of flow separation. The symmetric geometry (of the constriction) (symmetric about its center) (i.e., $n = 2$) is generally narrower in the converging part of the stenosis. So it induces an excess flow acceleration as compared to asymmetric stenosis ($n = 4$). The centre line velocity is seen to take a larger distance to recover its initial value as Reynolds number increases.

The wall shear stress is of physiological importance and there exist two contradictory hypothesis about its role in the initiation of atherosclerosis. No reliable method seems to be available for computing wall shear stress. In this situation, the numerical simulation provides some insight into the level of the wall shear stress involved. Fig.5 is the graphical representation of wall shear stress for symmetric ($n = 2$), slightly asymmetric ($n = 4$) and severely asymmetric ($n = 6$) stenoses at the Reynolds number $Re = 220$ for 51% area reduction (i.e., for $h = 0.3$). It is noticed that flow separates in case of severely asymmetric constriction ($n = 6$), flow separation starts in case of slightly asymmetric constriction ($n = 4$), but no separation takes place in case of symmetric constriction ($n = 2$).

Fig.6 illustrates the variation of wall shear stress along the solid as well as flexible surfaces for differently shaped constrictions at $Re = 600$ and for $h = 0.5$. It is seen that the location of the peak vorticity occurs just before the minimum constriction plane for both rigid and flexible wall models. The magnitude of the wall shear stress values increase rapidly when the flow approaches to the constriction and reaching a peak value near the minimum constriction plane in all cases. At a location downstream of this, the wall shear stress decreases rapidly and reverses to negative values when separation begins at the wall of the tube.

The places of zero vorticity are the locations of stagnation points as well as the separation and reattachment points of the attached vortices. It is also noted that the peak value of wall shear stress (in the converging part of the stenosis) decreases as the shape of a smooth stenosis changes and maximum wall shear stress is attained in case of a symmetric stenosis ($n=2$). This is in perfect conformity with the analytical study of Halder (1985). For both rigid and flexible arteries, an almost similar trend is observed in the respective distributions of wall shear stress differing in magnitudes only. Peak value of wall shear stress is maximum in case of rigid tube rather than that of flexible one. Here, the point of separation is shifted further towards downstream in case of rigid tube compared to that of flexible tube.

Fig.7 exhibits the effect of severity of the stenosis on both symmetric and asymmetric cases. Peak value of wall shear stress and the length of separation zone increase in both the cases as the height of the constriction increases.

In Fig.8, the distributions of wall shear stresses (τ_w) for the Reynolds numbers $Re = 600, 1000$ are given. At the highest Reynolds number considered, exactly the same situation occurs in the converging part of the stenosis, as shown in Fig.9(a). In the downstream diverging part, on the other hand, the deceleration of the fluid is more modest than at low Reynolds number and the axial velocity is still far from its asymptotic limit (2) at the downstream end of the stenosis in both symmetric and asymmetric cases. The length of separation increases in case of asymmetric constrictions and the point of separation and also the point of reattachment are shifted further towards downstream in those cases.

The fluctuation level in case of shear stress on the wall is also of considerable interest. It has been noted that highly variable wall shear stress can also result in a predilection toward atherosclerosis. The variability in shear stress can prevent endothelial cells from aligning in the direction of the flow, thereby making the intima more permeable to the entry of monocytes and lipoproteins. Oscillatory nature of wall shear stress at $Re=1000$ and $h=0.3$ is noticed in Fig.9(a). From this figure, it is very clear that oscillation in the shear layer appears earlier in case of asymmetric constriction than the symmetric constriction. Length of separation increases in case of asymmetric constrictions and the point of separation and also the point of reattachment are shifted further towards downstream in those cases.

The unsteady response of the flow phenomena through distensible artery seems to have major significance in realistic blood flow under stenotic condition. Keeping this in mind the behavior of stream wise velocity component with time for $Re = 600$, at $z = 11$ (where z is the distance from the inlet of the tube) (i.e., in the constricted region) for 51 % area reduction for asymmetric constriction ($n = 6$) for both rigid and flexible arteries is presented in Fig.9(b). Both the rigid and flexible arteries experience large distortions on stream wise velocity component at the onset of time followed by uniformly undulating stream wise velocity in case of rigid artery and an uniform stream wise velocity for the flexible one for rest of the time considered here.

In Fig.10(a), the oscillation in the stream wise velocity component with frequency 0.2 is noted at $z = 11$ (where z is the distance from the inlet of the tube) (i.e., in the constricted region) for $Re=1000$ for 51 % area reduction for asymmetric constriction ($n = 6$). In the upstream of the constriction, no oscillation is noticed. The time history of stream wise velocity component at $z = 24$ (i.e. where the constriction ends) for $Re = 1000$ and for 51% blockage for asymmetric constriction ($n = 6$) has been shown in Fig.10(b). The different type of oscillation but with same frequency is noticed.

The streamline patterns are shown in Fig.11(a), (b), (c) for symmetric ($n = 2$), slightly asymmetric ($n = 4$) and severely asymmetric ($n = 6$) constrictions respectively. These figures clearly exhibit the formation of separating bubbles after the constriction in each case. It is also noticed that the length of circulatory bubbles increases with the asymmetry of the constriction. Asymmetry constriction plays a vital role in flow separation.

5. Conclusion

A mathematical model of arterial flow through differently shaped stenosis is presented here. The comparison of the results of present study with the existing ones based on the Newtonian characterization of blood, the rigid artery and the steady state situation reveals good agreement and hence the present model would certainly give better insight into the complex flow phenomena in the stenotic conditions. Potential improvement over the previous models has been made by the incorporation of vessel wall distensibility and the effect of unsteadiness. The development of the separation zones towards the diverging section of the constriction is believed to be the prime areas for further deposition of atherosclerotic plaques. The role of asymmetry constriction in a realm of the arterial plaque may be useful for early detection of cardiovascular diseases.

Acknowledgement

One of the authors (G.C.L.) gratefully acknowledges the financial support of University Grants Commission, New Delhi, India [Project F. No. 30-244/2004(SR)] for pursuing this work. The authors are thankful to the honorable reviewers for constructive suggestions.

REFERENCES

- Ahmed, A.S. and Giddens, D. P. (1983). Velocity measurements in steady flow through axisymmetric stenosis at moderate Reynolds numbers, *J. Biomech.*, **16**, pp.505-516.
- Andersson, H.I., Halden, R. and Glomsaker, T. (2000). Effect of surface irregularities on flow resistance in differently shaped arterial stenoses, *J. Biomech.*, **33**, pp.1257-1262.
- Back, L.H., Cho, Y.I., Crawford, D.W., and Cuffel, R.F. (1984). Effects of mild atherosclerosis on flow resistance in a coronary artery casting of man, *ASME J. of Biomech. Eng.*, **106**, pp. 45-83.
- Chakravarty, S., Mandal, P.K. and Sarifuddin (2005). Effect of surface irregularities on unsteady pulsatile flow in a compliant artery, *Int. J. Nonlinear Mech.*, **40**, pp. 1268-1281.
- Deshpande, M.D., Giddens, D.P. and Mabon, R.F. (1976), Steady laminar flow through modeled vascular stenoses, *J. Biomech*, **9**, pp. 165-174.
- Fung, Y.C. (1981). *Biomechanics, Mechanical properties of living tissues*, Springer-Verlag, New York.
- Harlow, F.H. and Welch, J.E. (1965). Numerical calculation of time dependent viscous incompressible flow of fluid with free surface, *Phys. of Fluids*, **8**, pp. 2182-2189.
- Johnston, P.R. and Kilpatrick, D. (1991), Mathematical modeling of flow through an irregular arterial stenosis, *J. of Biomech.*, **24**, pp.1069-1077.
- Layek, G.C., Mukhopadhyay, S. and Samad, A.S. (2005). Oscillatory flow in a tube with multiple constrictions, *Int. J. of Fluid Mech. Research*, **32**, No.4, pp. 402-419.
- Lighthill, J., 1975. *Mathematical Biofluidynamics*, SIAM, Philadelphia.
- Misra, J.C. and Chakravarty, S. (1986). Flow in arteries in presence of stenosis, *J. Biomech.*, **19**, pp.907-918.

- Mittal, R., Simmons, S. P., and Udaykumar, H.S. (2001). Application of large-eddy simulation to the study of pulsatile flow in a modeled arterial stenosis, *J. of Biomech. Eng. ASME*, **123**, pp.325-332.
- Pedley, T.J. (1980). *The Fluid Mechanics of large blood vessels*, Cambridge University Press.
- Pontrelli, G. (2001). Blood flow through an axisymmetric stenosis, *Proceedings of the Institution of Mechanical Engineers, Part H: Journal of Engineering in Medicine*, 215, No.1, pp. 1-10.
- Roach, M.R. (1963). Change in arterial distensibility as a cause of poststenotic dilatation, *Am. J. Cardiol.*, **12**, pp.802-815.
- Young, D.F. (1979). Fluid mechanics of arterial stenosis, *J. Biomech. Engng., ASME*, **101**, pp.157-175.
- Young, D.F., and Tsai, F. Y. (1973), Flow characteristics in models of arterial stenoses-I, Steady flow, *J. Biomech.*, **6**, pp. 395-410.
- Young, D.F., and Tsai, F. Y. (1973). Flow characteristics in models of arterial stenoses-II, Steady flow, *J. Biomech.*, **6**, pp. 547-559.

Figure Captions

Fig.1(a) Geometry of the tube with symmetric as well as asymmetric constrictions.

Fig.1(b) Profile for irregular stenosis (Back, et al. (1984)).

Fig.2(a) Comparison of wall shear stresses for irregular model at Reynolds numbers $Re = 20$ and 1000.

Fig.2(b) Comparison of non dimensional pressure drop.

Fig.3 Pressure distribution along the wall in a tube with symmetric and asymmetric constriction of same height $h = 0.3$ and at $Re = 600$.

Fig.4 Centre line u-velocity in a tube with symmetric and asymmetric constriction of same height $h = 0.3$ at $Re = 600$.

Fig.5 Wall shear stress distribution in a tube with symmetric as well as asymmetric constrictions of same height $h = 0.3$ at $Re = 220$.

Fig.6 Wall shear stress distribution in a rigid as well as flexible tube with symmetric and asymmetric constrictions of same height $h = 0.5$ at $Re = 600$.

Fig.7 Comparison of wall shear stress in a tube with symmetric as well as asymmetric constrictions at $Re = 600$.

Fig.8 Comparison of wall shear stress in a tube with symmetric as well as asymmetric constrictions of same height $h = 0.3$.

Fig.9(a) Wall shear stress distribution in a tube with symmetric as well as asymmetric constrictions of same height $h = 0.3$ at $Re = 1000$.

Fig.9(b) Time history of stream wise velocity component at $Re = 600$ in a rigid as well as flexible tube with asymmetric constriction ($n = 6$) of height $h = 0.3$ at $z = 11$ (in the constricted region).

Fig.10(a) Time history of stream wise velocity component at $Re = 1000$ in a tube with asymmetric constriction ($n = 6$) of height $h = 0.3$ at $z = 11$ (in the constricted region).

Fig.10(b) Time history of stream wise velocity component at $Re = 1000$ in a tube with asymmetric constriction ($n = 6$) of height $h = 0.3$ at $z = 24$.

Fig.11(a) Streamlines in a tube with symmetric constriction of 75% area reduction at $Re = 600$.

Fig.11(b) Streamlines in a tube with asymmetric constriction ($n = 4$) of 75% area reduction at $Re = 600$.

Fig.11(c) Streamlines in a tube with asymmetric constriction ($n = 6$) of 75% area reduction at $Re = 600$.

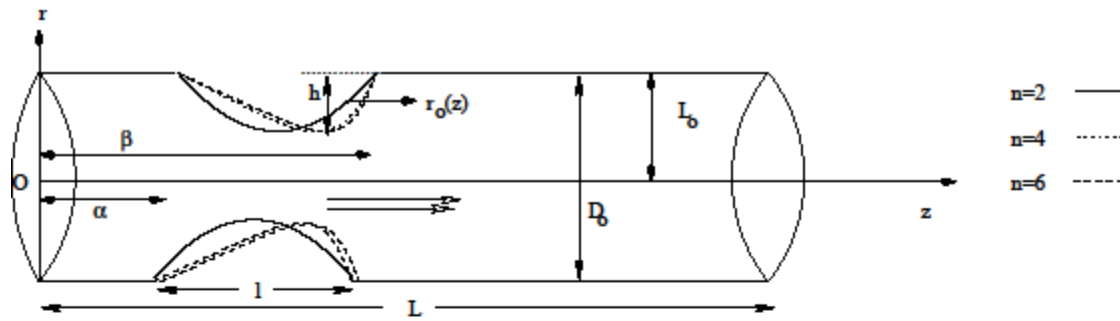


Fig.1(a): Geometry of the tube with symmetric as well as asymmetric constrictions.

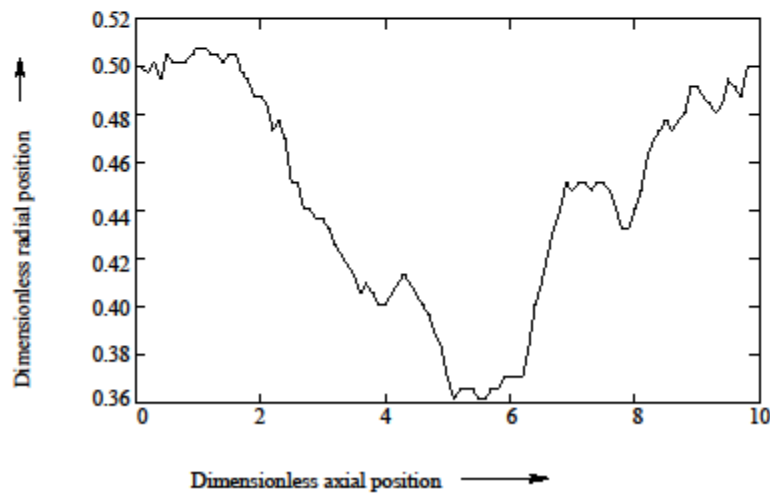


Fig.1(b): Profile of irregular stenosis (Back et. al., 1984)

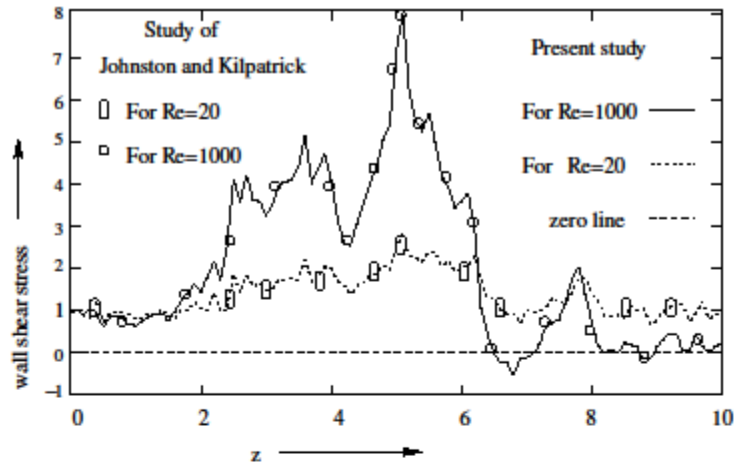


Fig.2(a): Comparison of wall shear stresses for irregular model at Reynolds numbers $Re=20$ and 1000.

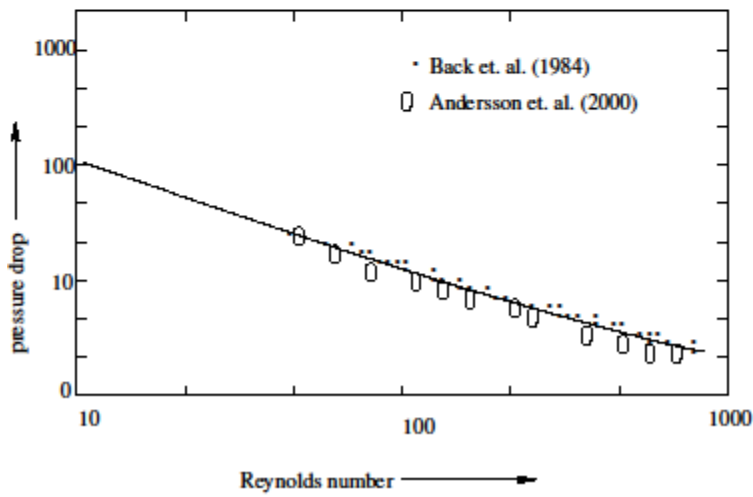


Fig.2(b): Comparison of nondimensional pressure drop.

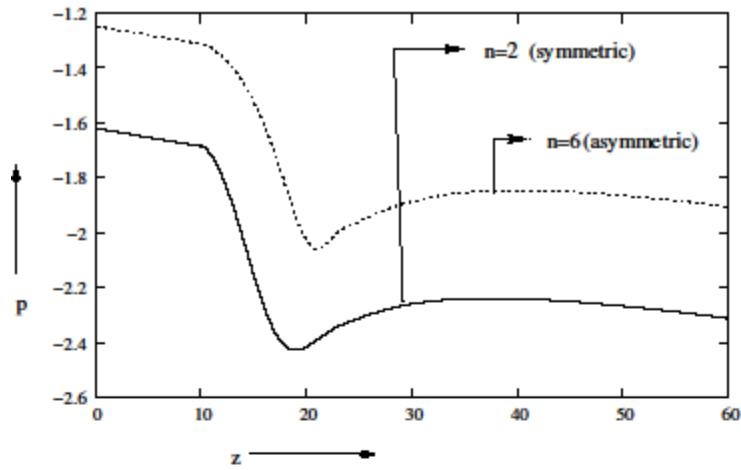


Fig.3: Pressure distribution along the wall in a tube with symmetric constriction and the same in case of asymmetric constriction of same height $h=0.3$ at $Re=600$.

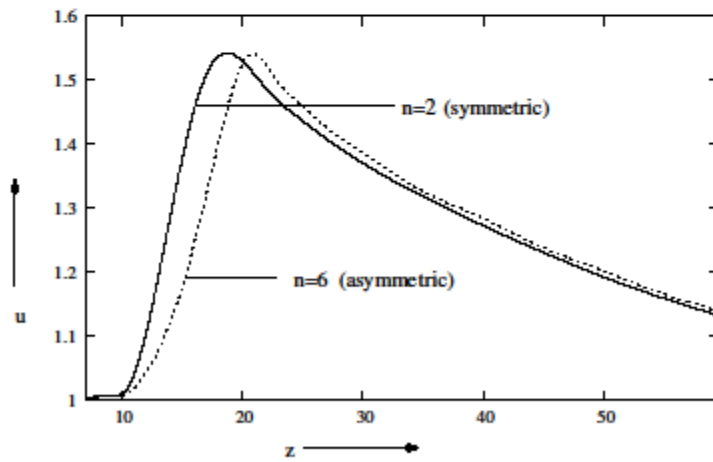


Fig.4: Centreline u -velocity in a tube with symmetric constriction and the same in case of asymmetric constriction of same height $h=0.3$ at $Re=600$.

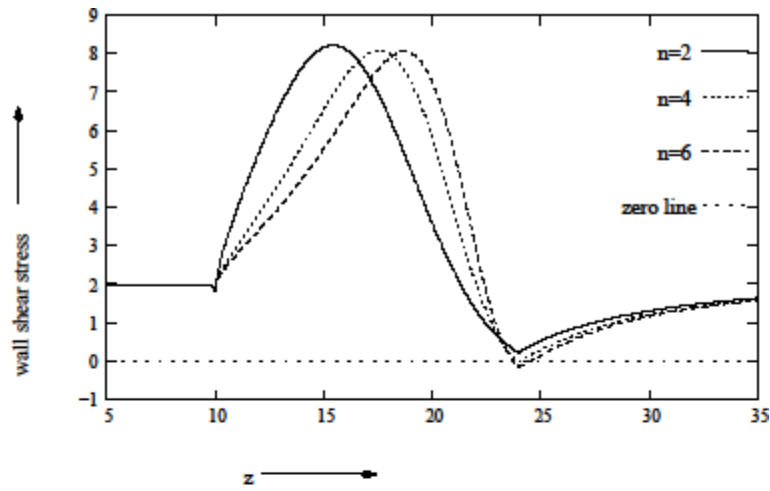


Fig. 5: Wall shear stress distribution in a tube with symmetric and asymmetric constrictions of same height $h=0.3$ at $Re=220$.

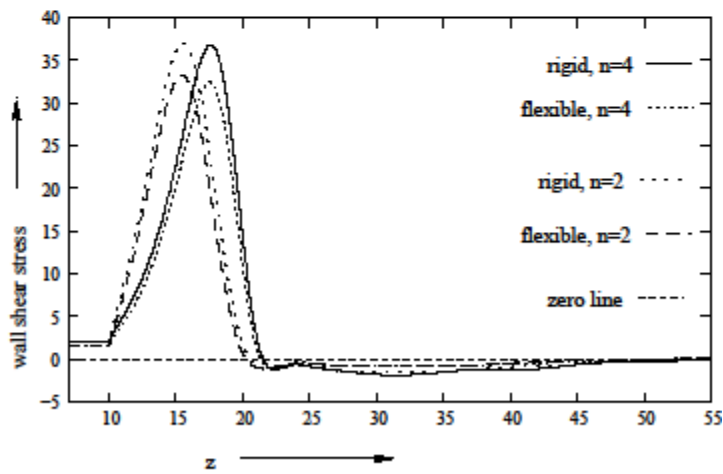


Fig. 6: Wall shear stress distribution in a rigid as well as flexible tube with symmetric and asymmetric constrictions of same height $h=0.5$ at $Re=600$.

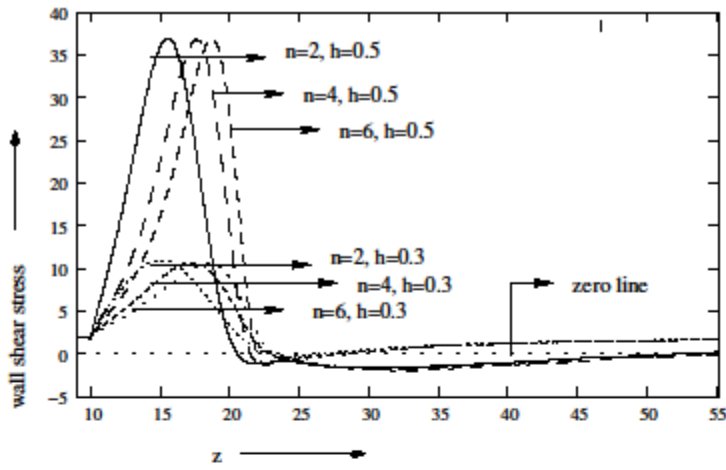


Fig. 7: Comparison of wall shear stress in a tube with symmetric and asymmetric constrictions at $Re=600$.

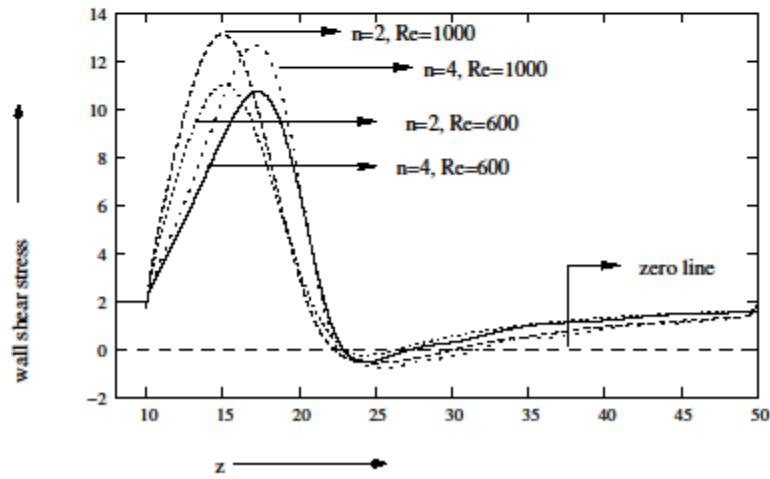


Fig.8 : Comparison of wall shear stress in a tube with symmetric and asymmetric constrictions of same height $h=0.3$.

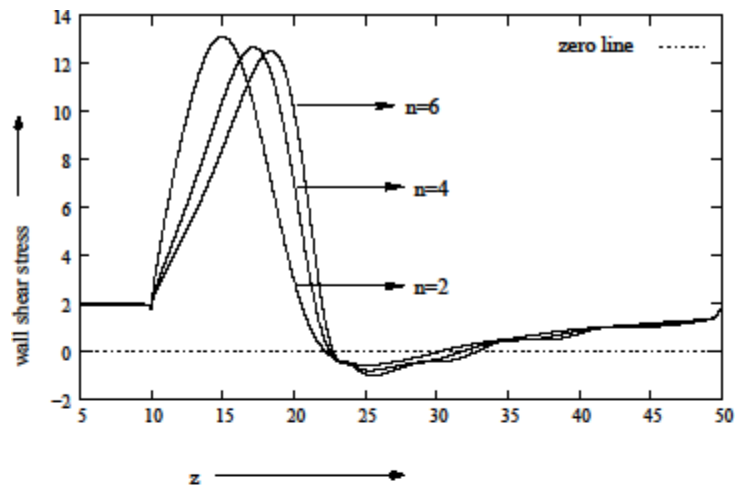


Fig.9(a) : Wall shear stress distribution in a tube with symmetric and asymmetric constrictions of same height $h=0.3$ at $Re=1000$.

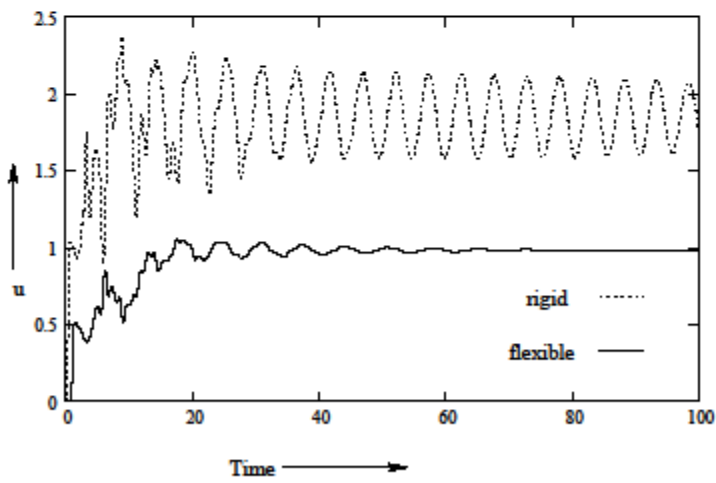


Fig.9(b): Time history of streamwise velocity component at $Re=600$ in a rigid as well as flexible tube with asymmetric constriction ($n=6$) of height $h=0.3$ at $z=11$ (in the constricted region).

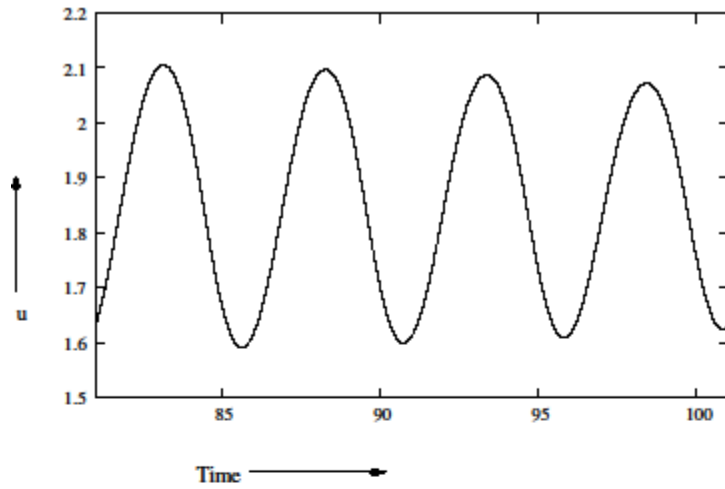


Fig.10(a) : Time history of streamwise velocity component at $Re=1000$ in a tube with asymmetric constriction ($n=6$) of height $h=0.3$ at $z=11$ (in the constricted region).

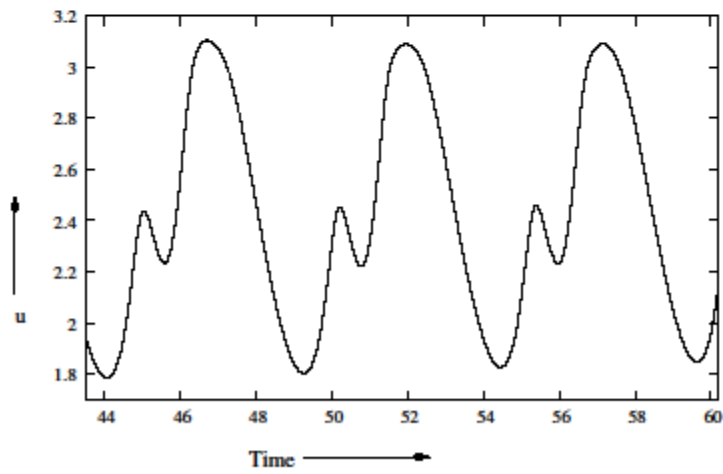


Fig. 10(b): Time history of streamwise velocity component at $Re=1000$ in a tube with asymmetric constriction ($n=6$) of height $h=0.3$ at $z= 24$.

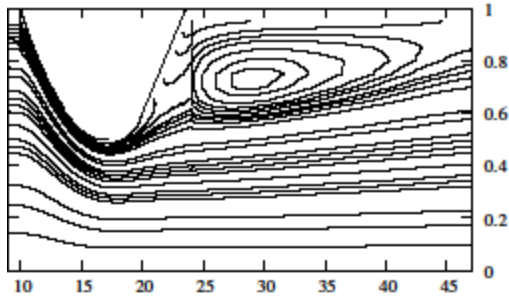


Fig.11(a) : Streamlines in a tube with symmetric constriction of 75% area reduction at $Re=600$.

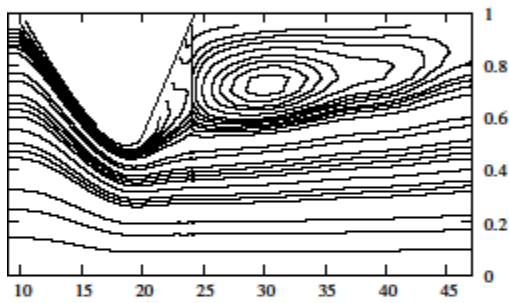


Fig.11(b) : Streamlines in a tube with asymmetric constriction ($n=4$) of 75% area reduction at $Re=600$.

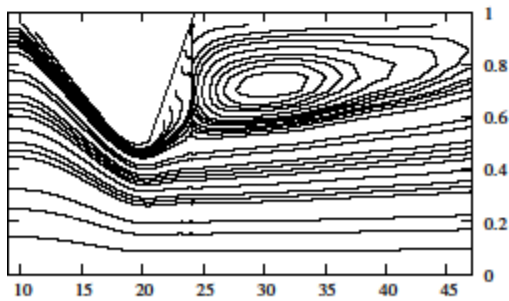


Fig.11(c) : Streamlines in a tube with asymmetric constriction ($n=6$) for 75% area reduction at $Re=600$.